Thickness dependent uniaxial magnetic anisotropy due to step-edges in (111)-oriented $La_{0.7}Sr_{0.3}MnO_3$ thin films

T. Bolstad, E. Lysne, U. L. Österberg, and T. Tybell[*]

T. Bolstad, E. Lysne, Prof. U. L. Österberg, and Prof. T. Tybell
Department of Electronic Systems, NTNU Norwegian University of Science and Technology, 7491 Trondheim, Norway

E-mail: thomas.tybell@ntnu.no

Abstract

The magnetic anisotropy of films of $La_{0.7}Sr_{0.3}MnO_3$ grown on vicinal (111)-oriented $SrTiO_3$ substrates are investigated. For temperatures above the tetragonal – cubic structural phase transition temperature of the substrate, a step edge induced uniaxial magnetic anisotropy is found at remanence, with a thickness-driven change in easy axis direction, from perpendicular to the step edges to parallel to the step edges with increasing thickness. The anisotropy constant for the investigated (111)-oriented samples is of the same magnitude as for previously reported (001)-oriented samples. The data is discussed in the framework of in-plane rotations of the oxygen octahedra resulting in a uniaxial anisotropy. Furthermore, the magnetic anisotropy is sensitive to the structural phase transition at 105K of the substrate, and the anisotropy constant increases drastically as the temperature is lowered below 105K.

Keywords: LSMO, magnetic anisotropy, step edges, (111)-orientation

1. Introduction

Magnetic anisotropy in thin films has extensively been studied for the last 60 years, and control of anisotropy opens for potential applications in electronic device technology [1]. Important magnetic characteristics such as coercive field, magnetization, and domain structure are in part controlled by the magnetic anisotropy. Thus, engineering of the magnetic anisotropy is central to the development of spintronic technology. For example, control of the magnetic anisotropy is essential in the realization of magnetic tunnel junctions. For such a device the resistance through the structure is controlled by the spin-orbit coupling at the interfaces, and hence the two ferromagnetic electrodes should ideally have different switching dynamics governed by the magnetic anisotropy [2]. Magnetic anisotropy control is also important for proposed devices based on domain wall movement such as racetrack memories [3]. Albeit large effort is focused on metallic systems, complex manganite oxides are interesting in this regard due to their strong coupling between functional properties and detailed atomistic structure [4]. $La_{0.7}Sr_{0.3}MnO_3$ (LSMO), especially, has received a significant amount of interest due to its robust room temperature ferromagnetism and a near 100 % spin polarization [5,6].

An experimental route to induce a magnetic anisotropy in thin films is to rely on stepped surfaces to break the magnetic symmetry. Step edges provide both a change in shape, and a vertical interface between film and substrate. The effects of step edges on perovskite oxides thin films have been extensively studied. In LSMO, magnetic anisotropy effected by step edges was first observed at 80 K in 13 nm thick films on highly vicinal, with a miscut of 10°, (001)-oriented $SrTiO_3$ (STO) (all crystallographic designations in this article are in the pseudo cubic symmetry) [7]. The steps edges were found to induce a uniaxial anisotropy with the easy axis parallel to the step edges. Later, the effect was also observed at room temperature in 7 nm and 25 nm thick films LSMO grown on STO(001) with very low vicinal angles of 0.13° and 0.24°,

respectively [8]. For lower temperatures and in thicker samples, the biaxial magnetocrystalline anisotropy is found to dominate [8,9], and the step density, i.e. vicinal angle, affects the thickness at which the uniaxial anisotropy disappears. For example, for a thickness of 120 nm, the uniaxial anisotropy is present in LSMO films grown on substrates with miscut angles larger than 4° [10].

A step and terrace surface are reported to affect different macroscopic properties. The magnetic switching is reported to proceed through nucleation and subsequent domain wall movement when the magnetic field is applied parallel to the step edges, and through coherent magnetization rotation when the field is applied perpendicular to the steps [7,11]. The magnetic anisotropy due to step edges are in $La_{1-x}Ca_xMnO_3$ observed to induce a measurable anisotropy in both transport and thermoelectric properties [12,13]. Anisotropic transport properties due to a step and terrace topology are also found in the double perovskite $LaBaCo_2O_{5.5+\delta}$ on STO [14]. For $Ba_{0.6}Sr_{0.4}TiO_3$ on MgO, step edges are found to induce structural antiphase boundaries [15]. By utilizing step edges in structural domain engineering in films of $BiFeO_3$ on STO, the ferroelectric coercive field can be lowered through the generation of nucleation sites at the steps [16]. The effect of step edges on magnetic anisotropy has also been explored in metallic ferromagnetic thin films [17-22]. For films of Co grown on Cu and Fe grown on Ag, the easy axis is seen to lie parallel to the step edges [17,20,21], while for Fe films on W, the easy axis is observed to lie either parallel or perpendicular to the step edges [18,19].

Advances in surface preparation techniques have recently enabled the exploration of (111)-oriented thin perovskite films [23,24]. By utilizing the (111) facet novel functionalities can be established such as polar metals [25], tunable exchange bias in a ferromagnet/paramagnet material system [26,27], and a ferrimagnetic state in an antiferromagnetic material at the

interface to a ferromagnet without charge transfer [28]. However, while the effects of control parameters such as step edges have been thoroughly investigated for (001)-oriented materials, data on the impact of step edges in (111)-oriented perovskite material systems is lacking. Due to the trigonal in-plane symmetry of (111)-oriented STO, thin films of LSMO on STO(111) assumes a rhombohedral unit cell with no macroscopic in-plane anisotropy at saturation magnetization [29], albeit a 6-fold symmetry microscopically in remanence [30]. This renders the LSMO/STO(111) system well suited for investigating the effects of step edges on the functional properties of (111)-oriented material systems. To this end, a small fields study of (111)-oriented LSMO is presented revealing subtle uniaxial anisotropy mechanisms due to the step edges, with the easy axis direction being parallel or not to the step-edges dependent on film thickness, in addition to sensitivity to structural phase transitions of the substrate. Thickness dependent step edge anisotropy has, to our knowledge, not been observed in (001)-oriented LSMO/STO systems, thus revealing how a change in crystalline thin film facet can influence subtle properties such as step-edge induced magnetic anisotropy.

2. Experimental and theoretical framework

LSMO thin films with thicknesses ranging from 9.5 nm to 40 nm were grown on (111)-oriented STO substrates (Shinkosha Co.,Ltd.) with a miscut angle in the range 0.05° - 0.15°. As the focus of this work is possible coupling of crystalline structure and magnetism, substrates with significantly differing miscut angles have not been used to rule out step-edge density driven effects. The miscut direction varied between each substrate. The films were deposited using a pulsed laser deposition (PLD) system. A KrF excimer laser with wavelength λ = 248 nm, fluence of ~2 J cm^{-2} and a repetition rate of 1 Hz was employed to ablate material from a stoichiometric LSMO target. The STO substrates were prepared by etching in buffered hydrofluoric acid for 45 seconds followed by annealing for one hour in oxygen flow at 1050 °C

resulting in atomically smooth step and terrace substrate [24]. During deposition the substrates were heated to 540 °C in a 0.35 mbar O_2 atmosphere with a distance of 45 mm from target to substrate, in order to ensure 2D growth [31]. The growth was monitored by reflection high-energy electron diffraction (RHEED), and after deposition the samples were cooled in a 100 mbar oxygen atmosphere.

The crystalline structure of the films was examined using a four-circle, high-resolution x-ray diffractometer (XRD, Bruker D8). In Figure 1 (a) a typical linear diffraction profile around the (111) reflections of STO and LSMO can be seen. The film thicknesses were determined from the thickness fringes. Rocking curves around the (111)-peak of LSMO reveal full width half maximum values of 0.035° and 0.04°, on the same order as for the substrates, indicating high quality films. Bulk LSMO has a rhombohedral unit cell (space group R-3c with lattice constant a = 5.471 Å and α = 60.43°), while STO is cubic at room temperature (space group Pm-3m with lattice constant a = 3.905). The low index in-plane directions for (111)-oriented LSMO are the $<1\bar{1}0>$ and $<11\bar{2}>$ family of directions and are illustrated in Figure 1 (b). The degree of strain relaxation was determined by linear scans of asymmetric substrate and film reflection peaks. For each sample, two reflections were studied, one with the in-plane component close to parallel to the step edges and one with the in-plane component close to perpendicular to the step edges. This was accomplished through finding the step edge directions relative to the sample edges by AFM, and utilizing this reference to align the step edges relative to the incoming x-rays. The investigated reflections belonged to the <114> or <312> families of reflections, however the exact reflection depended on the sample due to the varying miscut direction of the substrates. A reciprocal space map (RSM) of the 141 peak (in-plane component perpendicular to the step edges) of the 40 nm thick film is shown in Figure 1 (c). The reflections from the STO substrate and LSMO thin film are indicated in the figure. Linear scan profiles of the peaks along the out-

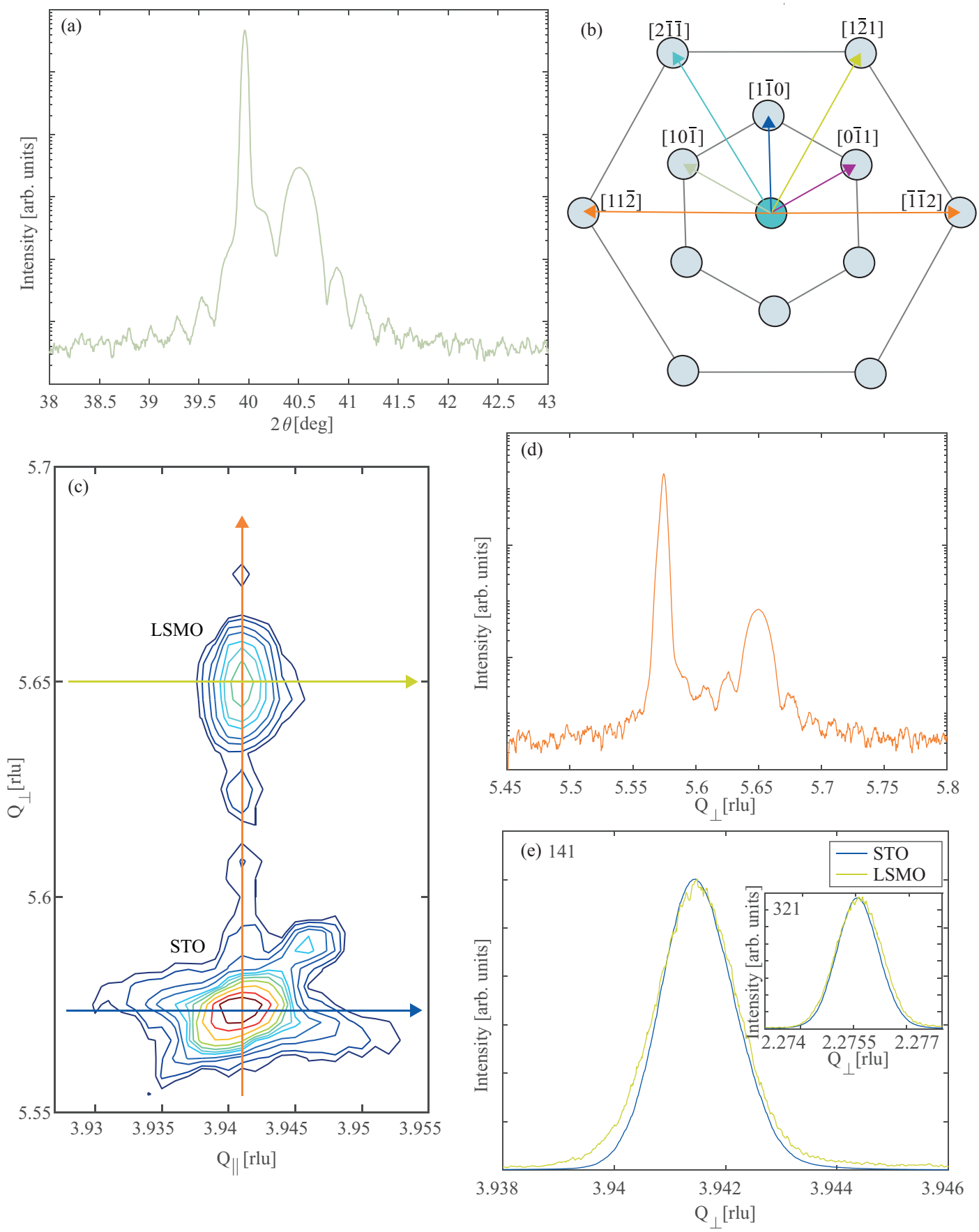

Figure 1: (a) A linear θ/2θ scan of the (111) peaks of 40 nm LSMO on STO. (b) A schematic of the atomic configuration of the (111) surface with the low index direction indicated. (c) A reciprocal space map of the 141 reflections of 40 nm LSMO on STO, with in-plane component perpendicular to the step edges. The orange arrow indicates the linear scan shown in Figure (d), while the yellow and blue arrows indicate the linear scans shown in Figure (e). The linear scans of the substrate and film 321 reflections, with in-plane component parallel to the step edges, is presented in the insert of (e).

of-plane and in-plane directions are shown in Figure 1 (d) and (e), respectively. As a comparison, the in-plane linear scan profiles of the 321 substrate and film reflections, with in-plane components parallel to the step edges, are shown in the insert of Figure 1 (e). It has previously been found that (111)-oriented LSMO on STO assumes a rhombohedral unit cell [29], which is consistent with the XRD results obtained in this study for all thicknesses. The RSMs for other in-plane directions and investigated film thicknesses are virtually identical, with the exception of a variation of the out-of-plane position in reciprocal space, $Q_{\perp}$, as a function of thickness. The in-plane relaxation of each film is obtained by comparing the in-plane positions in reciprocal space, $Q_{||}$, of the film and substrate reflections as illustrated in Figure 1 (e). A shift of the film peak towards higher values of $Q_{||}$ indicates a relaxation as bulk LSMO has a lower lattice parameter than STO. Surface characterization using atomic force microscopy (AFM, Veeco Nanoscope V) revealed a step and terrace structure with step heights of ~2.25 Å, consistent with the out-of-plane interplanar distance of ~2.22Å found from the XRD data. The LSMO thin films had similar surface roughness with a root mean square surface roughness of less than 0.2 nm for all samples.

The magnetic anisotropy was investigated using a magneto-optical Kerr effect setup in the longitudinal configuration (L-MOKE) at room temperature. Hysteresis measurements were obtained by applying a sinusoidal alternating magnetic field in the plane of the sample with amplitude 20 Oe and a frequency of 10 Hz. By rotating the sample around the surface normal of the sample, the magnetic response as a function of in-plane direction of the applied field was established. Additionally, the temperature dependency, between room temperature and 50K, of the magnetic properties was obtained using a vibrating sample magnetometer (VSM). In order to investigate temperature dependency of the anisotropy, the sample was rotated in increments

of 30° with the field aligned along the low index in-plane directions. In all cases, the anisotropy was probed by considering the magnetization in remanence, at zero applied external field.

In order to quantify the anisotropy, a general model for the energy of uniaxial anisotropy is used [32]:

$$\frac{E_a}{V} = K_u \sin^2(\theta - \varphi) \quad (1)$$

where E_a is the anisotropy energy, V is the volume of the sample, K_u is the uniaxial anisotropy constant, and φ is the direction of the easy axis. K_u can be determined by finding the anisotropy field, H_{an}, defined as

$$H_{an} = \frac{M_s}{(\mathrm{d}M/\mathrm{d}H)_{H=0}} \quad (2)$$

where M_s is the saturation magnetization and $\mathrm{d}M/\mathrm{d}H$ is the derivative of the magnetization with respect to the field for the hard axis at remanence. The uniaxial anisotropy constant is then found using

$$2K_u = \mu_0 H_{an} M_s \quad (3)$$

with μ_0 being the vacuum permeability. By using a model first proposed by Zener [33], and further developed by Carr [34], the temperature dependence of the anisotropy constant can be

modeled. The model assumes a ferromagnetic material with spontaneous magnetization produced by parallel spin alignment driven by exchange interactions, and temperature independent atomic coupling constants, resulting in, for uniaxial symmetry:

$$\frac{K_u(T)}{K_u(T_0)} = \left(\frac{M_s(T)}{M_s(T_0)}\right)^3 \quad (4)$$

with T being the temperature, and T_0 is a temperature below the Curie temperature. Here, T_0 is taken at 120 K due to the structural phase transition of the substrate at 105K, where STO undergoes a second order phase transition from cubic to tetragonal symmetry.

In the case of two perpendicular sources of anisotropy, the total anisotropy energy can be shown to be proportional to

$$\frac{E_a}{V} \propto \left|K_{u,1} - K_{u,2}\right| \sin^2(\theta) = K_u \sin^2(\theta) \quad (5)$$

where $K_{u,1}$ and $K_{u,2}$ are the anisotropy constants of the two sources of anisotropy and the resulting the easy axis will be dictated by the direction of the largest anisotropy constant. With two non-perpendicular anisotropies contributing, the resulting easy axis direction will lie between the two competing easy axes [35].

To investigate the role of unit cell symmetry, octahedral rotations and broken bonds as a source of magnetic anisotropy, the single ion model is utilized [36]. The energy of a single Mn-O bond is given by

$$E_i = -\frac{eQQ_2}{16\pi\varepsilon_0 R_i^3}(3cos^2\theta_i - 1) \quad (6)$$

where e is the electron charge, Q is the effective charge of the ligand, Q_2 is the quadrupole moment of the magnetic ion, ε_0 is the vacuum permittivity, R_i is the Mn-O bond length, and θ_i is the angle between the magnetization direction and the Mn-O bond. It has previously been found that QQ_2 is negative for LSMO [29]. E_i is summed over all bonds in a structure of eight (111)-oriented pseudo-cubic units with bonds broken along a plane perpendicular to the surface representing the step edge.

3. Results and discussion

In order to illustrate the step edge induced anisotropy in (111)-oriented LSMO, the details of two typical films, 19 nm and 40 nm thick, are presented. Figure 2 (a) and (b) show AFM micrographs of the two films, respectively, along with corresponding remanent magnetization as a function of azimuthal angle obtained by MOKE in Figure 2 (c) and (d). Both films exhibit a mainly uniaxial anisotropy, the 19 nm film with the easy axis perpendicular to the step edges, and the 40 nm film with the easy axis parallel to the step edges. The experimentally found anisotropy constants for the 19 nm and 40 nm films are shown in Figure 2 (e) and (f), respectively, along with the predicted temperature dependence from the model by Zener, showing good correspondence in the temperature range 110 K to 350 K. Below this range, the experimental value and theoretical values of K_u diverges sharply, indicating a change in the origin of the anisotropy linked to the structural changes in substrate at 105 K. The change of the easy axis direction relative to the step edges is further explored in Figure 3 (a) where the easy axis direction, as determined by MOKE, relative to the step edge direction as a function of film thickness is shown (blue open circles). An abrupt change in the relative direction of the

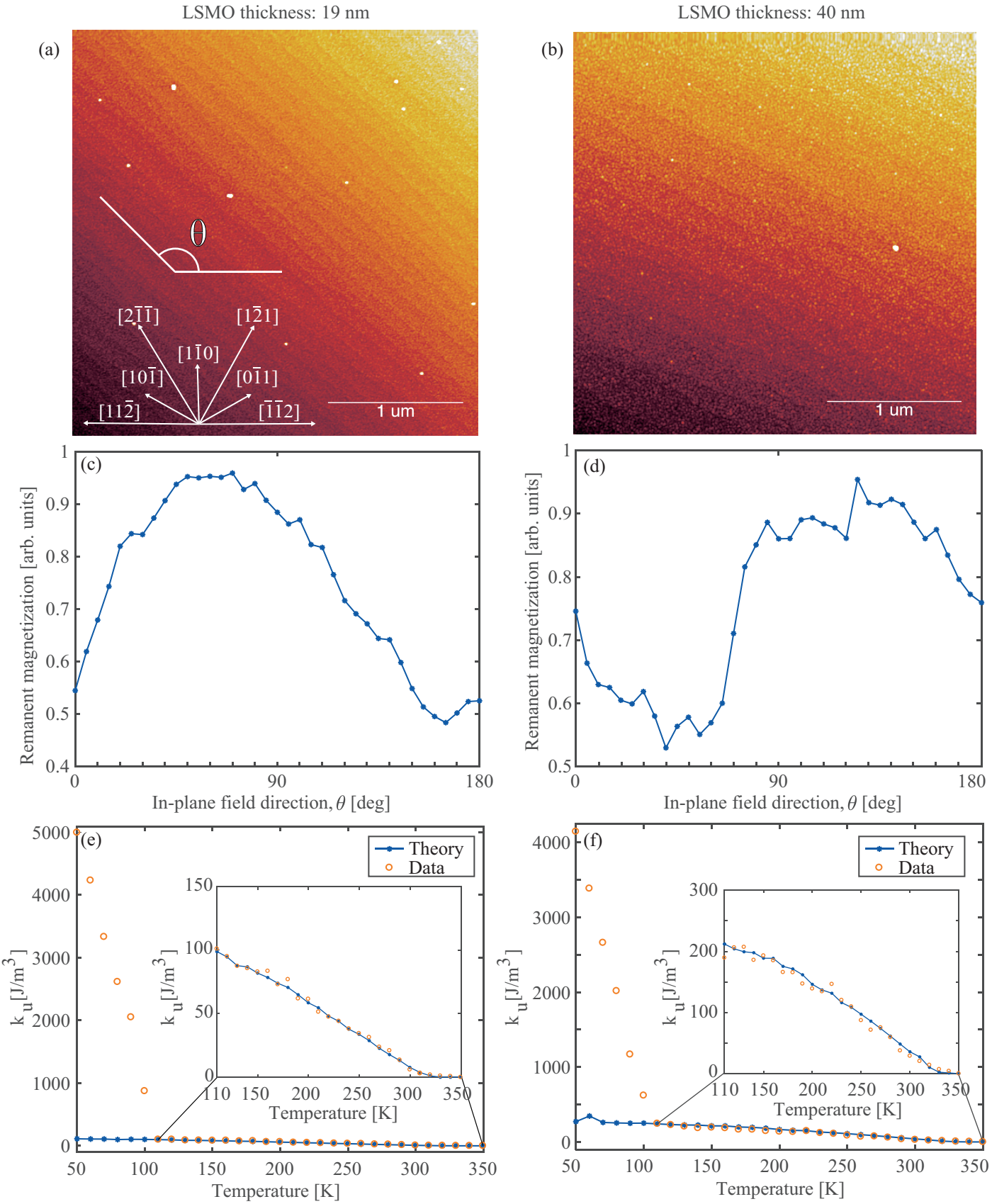

Figure 2: The top row shows AFM micrographs of a (a) 19 nm and (b) 40 nm LSMO film. The second row shows the remanent magnetization of the (c) 19 nm and (d) 40 nm LSMO film as a function of in-plane angle obtained by MOKE. The relation between the field angle and step edge is shown in Figure (a). In Figures (e) and (f) the anisotropy constants obtained by VSM for the 19 nm and 40 nm films, respectively, as functions of temperature is shown. The measured values are shown as open, orange circles and the theoretical values are shown as filled blue circles.

easy axis occurs around a film thickness of 20 nm. In the same figure the anisotropy constants measured at 120 K, for each film respectively, are presented by yellow stars, showing no dependence on thickness. The obtained values are all in the 100 J cm^{-3} – 300 J cm^{-3} range, except for the film with a thickness of 30.2 nm exhibiting a significantly higher value of the anisotropy constant. The observed uniaxial anisotropy constants are of the same size order as what is found for (001)-oriented LSMO on STO (~375 J cm^{-3} at 150 K for 7 nm and 18 nm thick films) [37]. The surface of the 30.2 nm thick sample was characterized by circular indentations, indicating poorer film quality, not observed for the other samples and this sample will not be focused on for the rest of this article.

The observed dependence of the anisotropy on step edge directions, points towards a step-induced anisotropy. There are several possibilities for this behavior, as reported in literature; shape anisotropy, uniaxial roughening at the interface, broken bonds or missing atoms at the steps, or strain relaxation either along or perpendicular to the step edges [20,38]. Both shape anisotropy and uniaxial interface roughening are interfacial effects, which would correspond to a decrease in K_u with increasing thickness [8]. In the thickness range investigated, no clear trend with thickness is observed and a rather constant anisotropy constant is obtained. This is not consistent with the primary cause of the anisotropy being an interface effect. Moreover, the single ion model gives that regardless of step edge direction the easy axis would be aligned parallel to the step edge, not consistent with the observed data. Hence, broken bonds are ruled out as main explanation to the changing anisotropy direction with film thickness.

One possible origin of the thickness dependent anisotropy direction is the presence of two competing, perpendicular anisotropies, $K_{u,1}$ and $K_{u,2}$, each dominant on different sides of the critical thickness. For example, a scenario could be constructed where an interface-induced

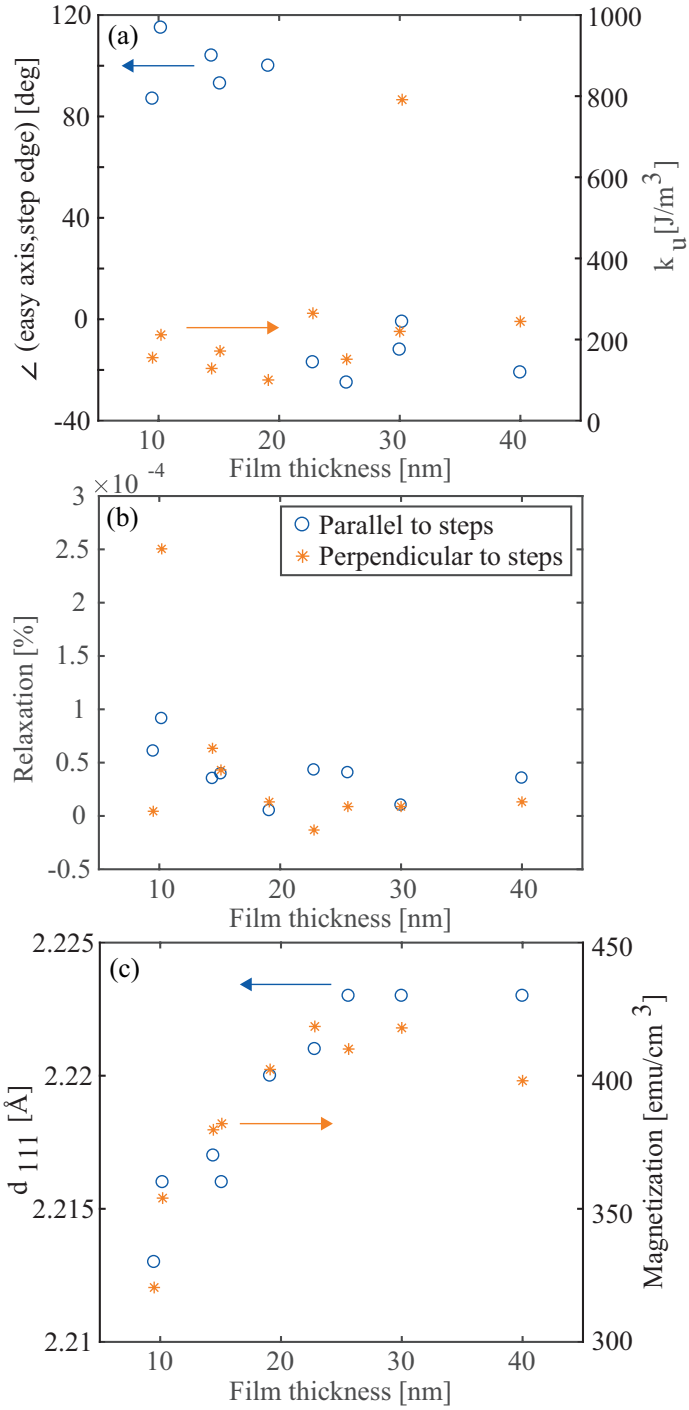

Figure 3: (a) The difference in direction between step edge and easy axis (blue, open circles) obtained by MOKE at room temperature and the anisotropy constant at 120 K (orange stars) obtained by VSM as a function of film thickness. (b) The degree of relaxation as a function of thickness parallel (blue circles) and perpendicular (orange stars) to the steps. (c) The out-of-plane parameter d_{111} (blue, open circles) and the remanent magnetization obtained by VSM at 120 K along the easy axis (orange stars) as functions of film thickness.

anisotropy with the easy axis perpendicular to the step edges competes with a bulk-induced anisotropy with the easy axis parallel to the step edges. The influence of the interface-induced anisotropy would then decrease with increasing film thickness relative to the bulk-induced anisotropy, shifting the observed easy axis from perpendicular to parallel at a critical thickness where $K_{u,1} = K_{u,2}$. However, in such a scenario the total anisotropy constant, $K_u = |K_{u,1} - K_{u,2}|$, would decrease towards the transition point where $K_{u,1} = K_{u,2}$ before increasing again below, a development not perceived in the presented data, see Figure 3 (a). The data hence points towards a change in the structure of the magnetization at the critical thickness instead of the simultaneous presence of two competing, perpendicular anisotropies.

In the single ion model, any in-plane structural perturbation, such as a change in atomic bond lengths from e.g. strain relaxation, can establish a source for magnetic anisotropy. The degree of strain relaxation, both along and perpendicular to the step edges, as a function of film thickness is depicted Figure 3 (b). In all samples, signs of micro relaxation were observed, with the film peak being shifted towards higher reciprocal lattice unit values as expected as LSMO has a smaller lattice constant than STO. However, no trend is observed with respect to thickness or direction relative to the step edges, nor to which of the high crystalline in-plane family of directions, <$1\bar{1}0$> or <$11\bar{2}$>, the relaxation was measured along. An estimate of the error is ± 2.5e-4 %, found by employing the full width half maximum of the relevant peak, larger than the measured relaxation.

The evolution of the out-of-plane parameter, d_{111}, along with the remanent moment along the easy axis at 120 K and obtained by VSM as a function of thickness is presented in **Figure 3 (c)**. Both values increase with thickness and saturates between a film thickness of 20 - 25 nm,

comparable to thickness where a change in the magnetic anisotropy direction is observed. For (001)-oriented LSMO straind to cubic $(LaAlO_3)_{0.3}$-$(Sr_2AlTaO_6)_{0.7}$, octahedral rotations are suggested to result in an uniaxial contribution to the biaxial magnetocrystalline anisotropy [39]. From the single ion model it can be shown that while a rhombohedral unit cell with an $a^-a^-a^-$ tilt pattern does not give an in-plane anisotropy, an infinitesimal deviation would, as stated earlier, give rise to a uniaxial anisotropy. Even though the XRD measurements are consistent with a rhombohedral unit cell for all thicknesses, a slight perturbation of the $a^-a^-a^-$ rotation pattern, below the XRD resolution, could hence result in an in-plane easy axis. The elongation of d_{111} with thickness affects the magnetic structure as seen from Figure 3 (c), where the remanent magnetization along the easy axis increases with d_{111}. As the in-plane lattice component is locked to the substrate, the change in magnetization does not occur due to bond elongation along the in-plane directions. Alternatively, the increase in magnetization with film thickness can originate from a change in the Mn-O-Mn bond angle due to a change in octahedral rotations. For example, in the single ion model any in-plane rotation of the oxygen octahedra parallel (perpendicular) the step edge direction will result in an easy axis perpendicular (parallel) to the rotation. We note that the observed decreased unit cell volume below 20 nm point towards an increase of the octahedral rotations to accommodate for the smaller volume present [40]. Hence, one possible interpretation of the presented data is a picture where non-symmetric octahedral rotations governs the magnetic easy axis, resulting from the change in out-of-plane parameter as the film thickness is reduced favoring in-plane octahedral rotations along the step edges. To further explore the role of octahedral rotations in the step edge induced anisotropy in these systems, octahedral rotation sensitive measurements should be performed, for example by synchrotron x-ray diffraction.

We now turn to the temperature dependence of the anisotropy constant. From the temperature evolution of the uniaxial anisotropy constant, Figures 2 (e,f), there is a change in anisotropy at the phase transition of STO. Figure 4 (a) depicts the remanent moment, measured by VSM, at 120 K and 50 K as a function of in-plane direction for the 19 nm film. While the observed anisotropy at 120 K, in the cubic phase of STO, confirms the uniaxial step edge anisotropy inferred from MOKE, at 50 K the easy axis direction changes. The remanent magnetization as

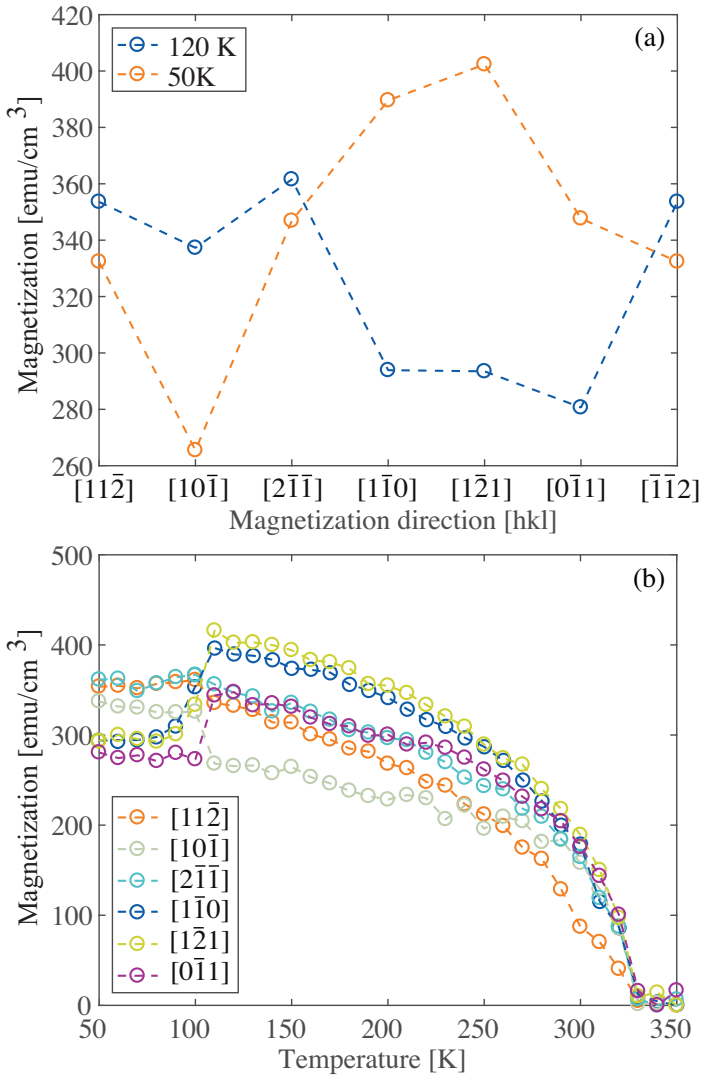

Figure 4: (a) The remanent moment of the 19 nm thick film as a function of magnetization direction obtained at 50 K and 120 K, with the STO substrate in the tetragonal and cubic phase, respectively. (b) The remanent magnetization field as a function of temperature and film thickness. The data in both figures were obtained by VSM.

a function of temperature and measurement direction for the 19 nm thick sample is shown in Figure 4 (b). A marked transition in the remanent magnetization is observed at the same temperature range as the change in K_u. The remanent magnetization along the $[11\bar{2}]$ and $[10\bar{1}]$ in-plane directions increase in the tetragonal phase of STO, while along the $[1\bar{1}0]$, $[1\bar{2}1]$, and $[0\bar{1}1]$ in-plane directions the remanent magnetization drops, as compared to the cubic phase of STO above 105K. In the case of the magnetization along $[2\bar{1}\bar{1}]$ the magnetization increases slightly when cooling from 110 K to 100 K, though not significantly more than at 10 K intervals at higher temperatures. The same trend is seen for all samples, however, the exact in-plane directions with increased and decreased remanent magnetization are sample dependent.

STO is reported to have structural domains in the tetragonal phase of STO [41]. The transition of STO from cubic to tetragonal involves an elongation along one of the <001> directions, which corresponds to an elongation along the $<11\bar{2}>$ in-plane directions for a (111)-surface. According to the single ion model of magnetic anisotropy, this results in a lower anisotropy energy along the direction of elongation for LSMO. In the tetragonal phase, the surface of STO is made up of a random pattern of twinned regions and large single-twin areas, which changes upon subsequent cooling and heating [41]. We speculate that this can give rise to a complex anisotropy at temperatures below 105 K, largely controlled by the interplay between step-induced anisotropy and magnetocrystalline anisotropy from the different structural domains. This is confirmed by repeated transitions through the phase transition, where it is observed that the remanent moment (along $[10\bar{1}]$) changes after run one, while the remanent moment in the cubic phase has a smaller variation (Figure 5 (a)). The moment in the tetragonal phase trends towards a saturation value, possibly due to a locking in of the structural domains. Although, the relation between the easy axis of each structural domain and the step edge direction can in principle be known, the macroscopic easy axis direction of the low temperature phase is

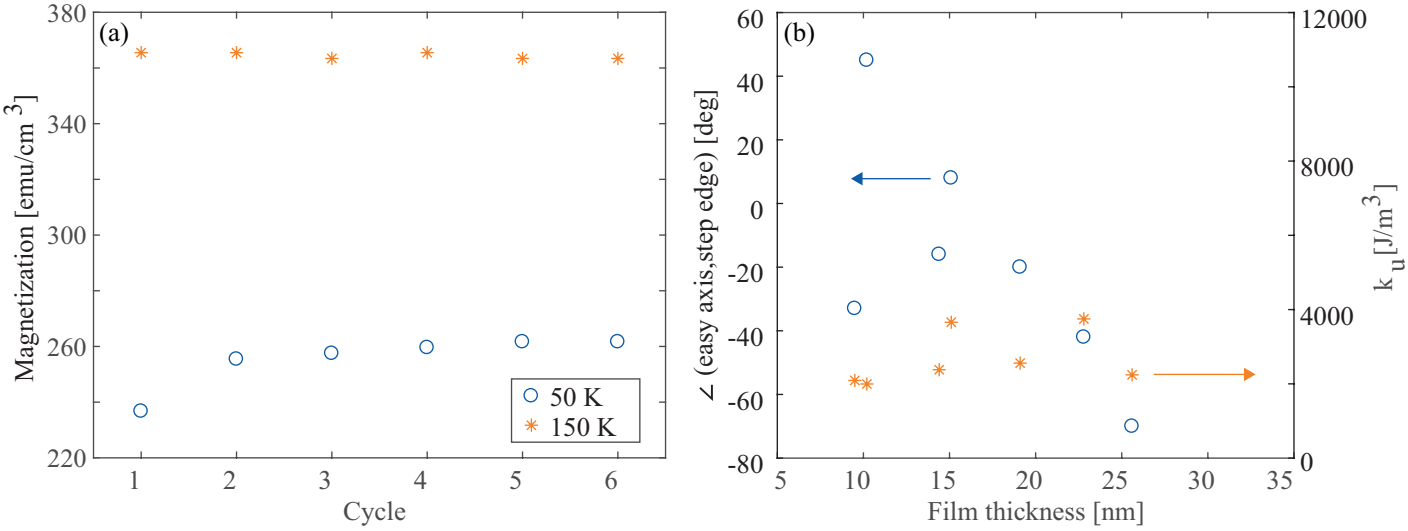

Figure 5: (a) The remanent magnetization of a 30 nm LSMO film at 50 K and 150 K upon repeated heating and cooling. (b) The difference between the easy angle direction and step edge direction (blue, open circles) and the anisotropy constant (orange stars) at 50 K as a function of film thickness. All data in this figure was obtained by VSM.

dependent on the exact domain distribution, and the value of K_u under 105 K is thus only an approximation (Figure 5 (b)). However, measuring along the different low index in-plane directions gives values of K_u of the same order.

In the tetragonal phase of STO the easy axis directions for all samples except the 10.4 nm thick film is less than 45° away from the step edge direction, as illustrated in Figure 5 (b). The experimentally obtained macroscopic easy axis at different angles to the step-edges is consistent with two non-perpendicular competing anisotropies; one contribution to the anisotropy given by the step edges, the other by magnetocrystalline effects with different directional contributions from different structural domains.

4. Conclusions

In conclusion, LSMO has been grown on (111)-oriented STO in a range of thicknesses from 9.5 nm to 40 nm in order to study the effect of vicinal substrates on magnetic anisotropy. We have shown that step edges induce a macroscopic uniaxial anisotropy with a thickness depended

easy axis above 105K; the easy axis lies perpendicular to the step edges for thin films, while for films thicker than a critical thickness the easy axis aligns parallel to the step edges. These results are consistent with the six-fold microscopic anisotropy observed in previous work on (111)-oriented LSMO [30]. Below 105 K, the effect of the substrate phase transition from a cubic to tetragonal unit cell results in a competition between step-edge contributions to the magnetic anisotropy and magnetocrystalline contributions from each crystalline domain, and hence no thickness transition is observed except for a varying magnetic easy-axis from sample to sample.

Acknowledgements

The Research Council of Norway is acknowledged for providing funding through Grant No. 231290.

References

[1] C. Wilts and F. Humphrey, *J. Appl. Phys.*, **1968**, 39, 1191.
[2] S. Peng, Y. Zhang, M. Wang, Y. Zhang, and W. Zhao, *Wiley Encyclopedia of Electrical and Electronics Engineering*, **2005**.
[3] S. S. Parkin, M. Hayashi, and L. Thomas, *Science*, **2008**, 320, 190.
[4] A. M. Haghiri-Gosnet and J. P. Renard, *J. Phys. D: Appl. Phys.*, **2003**, 36, R127.
[5] J. H. Park, E. Vescovo, H. J. Kim, C. Kwon, R. Ramesh, and T. Venkatesan, *Nature*, **1998**, 392, 794.
[6] M. Bowen, M. Bibes, A. Barthélémy, J.-P. Contour, A. Anane, Y. Lemaıtre, and A. Fert, *Appl. Phys. Lett.*, **2003**, 82, 233.
[7] Z.-H. Wang, G. Cristiani, and H.-U. Habermeier, *Appl. Phys. Lett.*, **2003**, 82, 3731.
[8] M. Mathews, F. M. Postma, J. C. Lodder, R. Jansen, G. Rijnders, and D. H. Blank, *Appl. Phys. Lett.*, **2005**, 87, 242507.
[9] S. Chaluvadi, P. Perna, F. Ajejas, J. Camarero, A. Pautrat, S. Flament, and L. Méchin, in J. Phys. Conf. Ser., Vol. 903, IOP Publishing, **2017**.
[10] P. Perna, C. Rodrigo, E. Jiménez, N. Mikuszeit, F. Teran, L. Méchin, J. Camarero, and R. Miranda, *J. Appl. Phys.*, **2011**, 109, 07B107.
[11] P. Perna, L. Méchin, M. Saib, J. Camarero, and S. Flament, *New J. Phys.*, **2010**, 12, 103033.
[12] L. Yu, Y. Wang, P. Zhang, and H.-U. Habermeier, *J. Cryst. Growth*, **2011**, 322, 41.
[13] H. Lu, C. Zhang, H. Guo, H. Gao, M. Liu, J. Liu, G. Collins, and C. Chen, *ACS Appl. Mater. Interfaces*, **2010**, 2, 2496.
[14] Q. Zou, M. Liu, G. Wang, H. Lu, T. Yang, H. Guo, C. Ma, X. Xu, M. Zhang, and J. Jiang, *ACS Appl. Mater. Interfaces*, **2014**, 6, 6704.
[15] J. Jiang, Y. Lin, C. Chen, C. Chu, and E. Meletis, *J. Appl. Phys.*, **2002**, 91, 3188.
[16] V. Shelke, D. Mazumdar, G. Srinivasan, A. Kumar, S. Jesse, S. Kalinin, A. Baddorf, and A. Gupta, *Adv. Mater.*, **2011**, 23, 669.
[17] A. Berger, U. Linke, and H. Oepen, *Phys. Rev. Lett.*, **1992**, 68, 839.
[18] J. Chen and J. Erskine, *Phys. Rev. Lett.*, **1992**, 68, 1212.

[19] H. J. Choi, Z. Qiu, J. Pearson, J. Jiang, D. Li, and S. Bader, *Phys. Rev. B*, **1998**, 57, R12713.
[20] D. Chuang, C. Ballentine, and R. O'Handley, *Phys. Rev. B*, **1994**, 49, 15084.
[21] R. Kawakami, E. J. Escorcia-Aparicio, and Z. Qiu, *Phys. Rev. Lett.*, **1996**, 77, 2570.
[22] H. C. Mireles and J. Erskine, *J. Appl. Phys.*, **2003**, 93, 7139.
[23] J. Chang, Y.-S. Park, and S.-K. Kim, *Appl. Phys. Lett.*, **2008**, 92, 152910.
[24] I. Hallsteinsen, M. Nord, T. Bolstad, P.-E. Vullum, J. E. Boschker, P. Longo, R. Takahashi, R. Holmestad, M. Lippmaa, and T. Tybell, *Cryst. Growth Des.*, **2016**, 16, 2357.
[25] T. H. Kim, D. Puggioni, Y. Yuan, L. Xie, H. Zhou, N. Campbell, P. J. Ryan, Y. Choi, J. W. Kim, J. R. Patzner, S. Ryu, J. P. Podkaminer, J. Irwin, Y. Ma, C. J. Fennie, M. S. Rzchowski, X. Q. Pan, V. Gopalan, J. M. Rondinelli, and C. B. Eom, *Nature*, **2016**, 533.
[26] M. Gibert, M. Viret, P. Zubko, N. Jaouen, J. M. Tonnerre, A. Torres-Pardo, S. Catalano, A. Gloter, O. Stephan, and J. M. Triscone, *Nature Communication*, **2016**, 7.
[27] M. Gibert, P. Zubko, R. Scherwitzl, J. Íñiguez, and J.-M. Triscone, *Nature Materials*, **2012**, 11.
[28] I. Hallsteinsen, M. Moreau, A. Grutter, M. Nord, P. E. Vullum, D. A. Gilbert, T. Bolstad, J. K. Grepstad, R. Holmestad, S. M. Selbach, A. T. N'Diaye, B. J. Kirby, E. Arenholz, and T. Tybell, *Phys. Rev. B*, **2016**, 94.
[29] T. Bolstad, E. Lysne, I. Hallsteinsen, E. Arenholz, U. L. Oesterberg, and T. Tybell, *J. Phys.: Condens. Matter*, **2018**, 30, 255702.
[30] I. Hallsteinsen, E. Folven, F. K. Olsen, R. V. Chopdekar, M. S. Rzchowski, C. B. Eom, J. K. Grepstad, and T. Tybell, *APL Mater.*, **2015**, 3, 062501.
[31] I. Hallsteinsen, J. E. Boschker, M. Nord, S. Lee, M. Rzchowski, P. E. Vullum, J. K. Grepstad, R. Holmestad, C. B. Eom, and T. Tybell, *J. Appl. Phys.*, **2013**, 113, 183512.
[32] S. Chikazumi and C. D. Graham, *Physics of Ferromagnetism 2e*. (Oxford University Press on Demand, 2009).
[33] C. Zener, *Phys. Rev.*, **1954**, 96, 1335.
[34] W. Carr Jr, *Phys. Rev.*, **1958**, 109, 1971.
[35] B. D. Cullity and C. D. Graham, *Introduction to Magnetic Materials*. (John Wiley & Sons, 2011).
[36] R. Skomski, *Simple Models of Magnetism*. (Oxford University Press on Demand, Oxford, 2008).
[37] M. Mathews, Doctoral dissertation, University of Twente, 2007.
[38] R. Arias and D. Mills, *Phys. Rev. B*, **1999**, 59, 11871.
[39] H. Boschker, M. Mathews, P. Brinks, E. Houwman, A. Vailionis, G. Koster, D. H. A. Blank, and G. Rijnders, *J. Magn. Magn. Mater.*, **2011**, 323, 2632.
[40] G. A. Samara, T. Sakudo, and K. Yoshimitsu, *Phys. Rev. Lett.*, **1975**, 35.
[41] A. Buckley, J. P. Rivera, and E. K. H. Salje, *J. Appl. Phys.*, **1999**, 86, 1653.